# Constructing the Near field and Far field with Reactive Metagratings: Study on the Degrees of Freedom

Vladislav Popov,[1,*] Fabrice Boust,[1,2] and Shah Nawaz Burokur[3]

[1] *SONDRA, CentraleSupélec, Université Paris-Saclay, 91190 Gif-sur-Yvette, France*

[2] *DEMR, ONERA, Université Paris-Saclay, 91123 Palaiseau, France*

[3] *LEME, UPL, Université Paris Nanterre, 92410 Ville d'Avray, France*

(Received 16 October 2018; revised manuscript received 28 January 2019; published 28 February 2019)

We report that metamaterial-inspired one-dimensional gratings (or metagratings) can be used to control nonpropagating diffraction orders as well as propagating ones. By accurate engineering of the near field, it becomes possible to satisfy power-conservation conditions and achieve perfect control over all propagating diffraction orders with passive and lossless metagratings. We show that each propagating diffraction order requires 2 degrees of freedom represented by passive and lossless loaded thin "wires." This provides a solution to the old problem of power management between diffraction orders created by a grating. The theory developed is verified by both three-dimensional full-wave numerical simulations and experimental measurements, and can be readily applied to the design of wavefront-manipulation devices over the entire electromagnetic spectrum as well as in different fields of physics.

DOI: 10.1103/PhysRevApplied.11.024074

## I. INTRODUCTION

At the beginning of the 20th century, the problem of intensity distribution among different diffraction orders produced by a diffraction grating was one of the most important in optics [1]. Since then, a particular class of gratings maximizing the intensity in a given diffraction order referred to as "blazed gratings" have been studied in detail [1–4] and perfect blazing was demonstrated in a nonspecular direction when only two orders propagate [5,6]. In the context of antenna applications, highly efficient reflection and transmission at small diffraction angles was achieved by means of classical reflectarrays and transmitarrays [7–9].

Amazing possibilities in manipulation of electromagnetic fields with engineered dense distributions of scatterers (metamaterials) have been demonstrated in the last two decades [10–13]. Extensive research in the area of metasurfaces, thin two-dimensional (2D) metamaterials, established a rigorous theoretical approach to arbitrarily control reflection and refraction of an incident plane wave [14–17]. In what follows we discuss examples of the perfect control (without spurious scattering) of the reflection and transmission that were demonstrated by means of a rigorous theory. Perfect refraction in the first diffraction order and beam splitting in transmission with equal excitation of the negative and positive first diffraction orders by means of passive and lossless bianisotropic metasurfaces was presented in Refs. [18–20] and Ref. [21], respectively. To perform perfect nonspecular reflection with passive and lossless metasurfaces, auxiliary surface waves have to be additionally excited [21–24]. Although it seems possible to design such metasurfaces, the design procedure is still not well established [23,24]. Huygens metasurfaces having equivalent electric and magnetic responses allow one to efficiently control diffraction from microwave frequencies [15] to optical frequencies [25] under the conditions of local normal power-flow conservation and conjugate impedance matching [26].

Ra'di *et al.* [27] recently introduced the concept of metagratings, which are an evolution of conventional one-dimensional diffraction gratings. The prefix "meta" implies that the grating is constructed from meta-atoms whose scattering properties can be judiciously engineered. Traditionally, in one-dimensional gratings there is a profile modulation in one direction and a translational symmetry in the other. In metagratings, the translation-invariant direction is engineered at a scale that is small compared with the wavelength such that it becomes possible to define an averaged macroscopic quantity such as an impedance density [28]. The possibility to engineer the impedance density and an accurate analytical model allows one to overcome the limitations of metasurfaces. For instance, by means of theory and full-wave simulations, the possibility of perfect nonspecular reflection and beam splitting in reflection with a metagrating composed of only a single

*physics.vlad@gmail.com

 

unit cell per period was demonstrated [27–29]. To realize perfect refraction in the first diffraction order three unit cells per period are required, as shown analytically in Ref. [30]. Lately, experimental verification of perfect reflection in the negative first diffraction order was reported by Rabinovich *et al.* [31]. Wong *et al.* [32,33] numerically and experimentally demonstrated efficient broadband nonspecular reflection with a two-cell periodic structure capable of controlling two propagating diffraction orders.

The way toward control over an arbitrary number of propagating diffraction orders by means of metagratings based on many unit cells was outlined in Ref. [34] for a reflection configuration. Moreover, it was shown that when the number of degrees of freedom is equal to the number of propagating diffraction orders, perfect total control is possible only in the case when engineered active and lossy responses are available. Otherwise, there are scattering losses. In this paper, we report that metagratings can be used to control nonpropagating diffraction orders as well as propagating ones. By accurate engineering of the near field it becomes possible to satisfy power-conservation conditions and achieve perfect control over all propagating diffraction orders with passive and lossless metagratings. In what follows, we study theoretically and validate experimentally the number of degrees of freedom required by each propagating diffraction order, thus providing a solution to the old problem of power management between diffraction orders created by a grating.

## II. PERFECT CONTROL OF DIFFRACTION: TWO REACTIVE ELEMENTS PER ORDER

Theoretically, a metagrating is described as a one-dimensional periodic array of polarization line currents that are excited in thin loaded "wires" by a TE-polarized plane wave incident at an angle $\theta$ and having the electric field along the wires. We consider a reflective-type metagrating when the wires are placed on top of a perfect-electric-conductor- (PEC)backed dielectric substrate. A schematic of the system under consideration is depicted in Fig. 1 (a). A grounded substrate should be carefully chosen to provide efficient excitation of line currents [i.e., $h \approx \lambda/(4\sqrt{\varepsilon_s\mu_s - \sin\theta^2})$] and avoid excitation of waveguide modes [34].

Since the illuminated structure is periodic, the wave reflected outside the substrate [$z < -h$] can be represented as a superposition of plane waves $\sum_{m=-\infty}^{+\infty} A_m^{\mathrm{TE}} e^{-i\xi_m y + i\beta_m z}$. The plane waves have tangential and normal components of the wave vector of $\xi_m = k\sin\theta + 2\pi m/L$ and $\beta_m = \sqrt{k^2 - \xi_m^2}$, respectively, with $k$ being the wavenumber outside the substrate. A simple model of metagratings allows one to find the amplitudes $A_m^{\mathrm{TE}}$ analytically (see details in Appendix A):

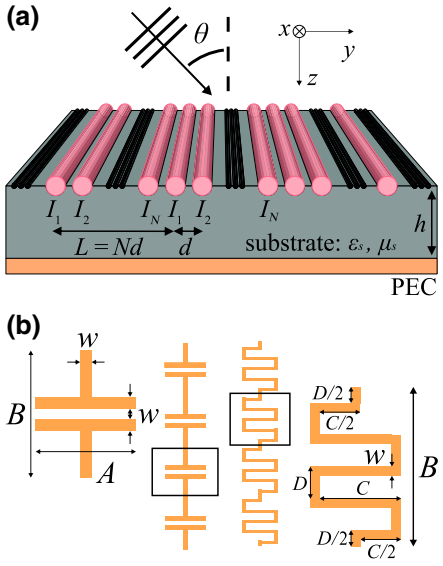


FIG. 1. The physical system considered and elements of its practical implementation. (a) System under consideration: a periodic array of thin wires (large cylinders) placed on a PEC-backed dielectric substrate having relative permittivity $\varepsilon_s$, permeability $\mu_s$, and thickness $h$. The array is excited by a TE-polarized plane wave incident at an angle $\theta$. (b) Implementation at microwave frequencies of capacitively loaded (left) and inductively loaded (right) PEC strips.

$$A_m^{\mathrm{TE}} = -\frac{k\eta}{2L}\frac{(1+R_m^{\mathrm{TE}})e^{i\beta_m h}}{\beta_m}\sum_{q=1}^{N} I_q e^{i\xi_m(q-1)d} + \delta_{m0}R_0^{\mathrm{TE}}e^{2i\beta_0 h}, \tag{1}$$

where $\eta = \sqrt{\mu/\varepsilon}$ is the characteristic impedance outside the substrate, $\delta_{m0}$ represents the reflection of the incident wave from the grounded substrate, and $R_m^{\mathrm{TE}}$ is the Fresnel reflection coefficient. Equation (1) reveals that each of the $N$ line currents in a supercell contributes to the reflected plane waves through the discrete Fourier transformation of the sequence $I_q$. Although there is an infinity of reflected plane waves, only a finite number $M = r + l + 1$ of them are scattered in the far field, determining the diffraction pattern. $r$ and $l$ are the largest integers such that $\beta_r > 0$ and $\beta_{-l} > 0$. Currents $I_q$ represent degrees of freedom that can be harnessed to control the amplitudes of the reflected fields as seen from Eq. (1).

Each polarization line current is excited in a thin wire characterized by its input-impedance density $Z_{\mathrm{in}}$ and load-impedance density $Z_q$. Necessary currents $I_q$ can be obtained by the loading of wires with suitable load-impedance densities $Z_q$, which are found from the

following equation:

$$Z_q I_q = E_q^{(\mathrm{exc})} - Z_{\mathrm{in}} I_q - \sum_{p=1}^{N} Z_{qp}^{(m)} I_p. \tag{2}$$

The right-hand side of Eq. (2) represents the total electric field at the location of the $q$th wire, where $E_q^{(\mathrm{exc})}$ represents the excitation field (incident wave plus the wave reflected from the grounded substrate) and $Z_{qp}^{(m)}$ are the mutual-impedance densities that account for the interaction between the wires and between the wires and the grounded substrate. Details on the derivation of Eqs. (1) and (2) as well as the explicit expressions for the impedance densities can be found in Ref. [34]. For the reader's convenience, we provide the main parts of the derivations in Appendix A.

Total control of the diffraction pattern is possible by $M$ line currents per supercell. However, we are particularly interested in purely reactive solutions of Eq. (2), since in practice it can be challenging to engineer active and/or lossy response of the load. Thus, the currents $I_q$ should also satisfy the conditions of passivity and absence of loss:

$$\mathrm{Re}\left[\left(E_q^{(\mathrm{exc})} - \sum_{p=1}^{N} Z_{qp}^{(m)} I_p\right) I_q^*\right] = \mathrm{Re}(Z_{\mathrm{in}})|I_q|^2, \tag{3}$$

where the asterisk stands for the complex conjugate. Equation (3) represents a set of $N$ quadratic algebraic equations with the real and imaginary parts of currents being the variables and simply means that the $q$th current radiates all the power expended on its excitation. Additional $M$ (complex-valued) line currents are required to satisfy Eq. (3). Thus, $N = 2M$ line currents per supercell are necessary to establish arbitrary diffraction patterns exactly. Although there can be many line currents in a period, the distance between them is on the order of $\lambda/4$ ($\lambda$ is the operating wavelength), which does not allow one to perform homogenization and introduce surface impedance.

From the physical point of view, the additional $M$ currents are used to set the amplitudes $A_m^{\mathrm{TE}}$ of the surface waves (or nonpropagating diffraction orders, $m > r$ and $m < -l$) that would guarantee satisfaction of Eq. (3). For better understanding, we consider an example of perfect reflection in the first diffraction diffraction order of a plane wave at normal incidence ($r = l = 1$). In this case, one has to cancel two propagating diffraction orders since there are three plane waves reflected in the far field, and thus the necessary number $N$ of line currents per period is six. First, one sets the amplitudes of the plane waves in the far field as $A_{-1}^{\mathrm{TE}} = 0$, $A_0^{\mathrm{TE}} = 0$, and $A_1^{\mathrm{TE}} = e^{i\phi_1}$, where $\phi_1$ is the phase of the anomalously reflected wave. Then the line currents $I_q$ ($q = 1, 2, \ldots, 6$) found from Eq. (1) ($m = -3, -2, \ldots, 2$) are substituted into Eq. (3). The unknown (complex) amplitudes $A_{-3}^{\mathrm{TE}}$, $A_{-2}^{\mathrm{TE}}$, and $A_2^{\mathrm{TE}}$ of the surface waves are found by our solving Eq. (3), what automatically guaranties the passive and lossless load-impedance densities $Z_q$ calculated afterward from Eq. (2).

## III. DESIGN, SIMULATION, AND EXPERIMENT

Once the necessary load-impedance densities are known, one has to come up with a practical implementation of the loads. In a general case, capacitive and inductive loads are required for such design implementation. As a proof of concept we demonstrate the design procedure for metagratings operating at microwave frequencies near 10 GHz. Thin metallic wires are realized as PEC strips having input-impedance density $Z_{\mathrm{in}} = k\eta H_0^{(2)}(kw/4)/4$, with $H_0^{(2)}$ being the Hankel function of the second kind and $w$ being the width of the strips. Capacitive and inductive responses can be achieved with the printed microstrip capacitors and inductors schematically shown in Fig. 1(b). The load-impedance density $Z_c$ of the printed capacitors can be approximately calculated by means of analytical formulas for the grid impedance of a PEC-strip capacitive grid [35–37]:

$$Z_c = -i\kappa_c \frac{\eta_{\mathrm{eff}}}{2A\alpha}, \quad \alpha = \frac{k_{\mathrm{eff}} B}{\pi} \ln\left(\frac{1}{\sin\left(\frac{\pi w}{2B}\right)}\right), \tag{4}$$

where $A$ is the length of the arms, $\eta_{\mathrm{eff}} = \eta/\sqrt{\varepsilon_{\mathrm{eff}}}$, $k_{\mathrm{eff}} = k\sqrt{\varepsilon_{\mathrm{eff}}}$, $\varepsilon_{\mathrm{eff}} = (1 + \varepsilon_s)/2$, $\alpha$ is the grid parameter, and $B$ is the period along the $x$ direction. The preceding expressions (4) were used in the context of metagratings (see, e.g., Refs. [29,34]). Since PEC strips act intrinsically as inductors themselves ($\mathrm{Im}[Z_{\mathrm{in}}] > 0$), the inductive load can be implemented by modulation of the effective length of the strip through a meandering design process [37,38]. Then, the inductive-load-impedance density $Z_i$ can be estimated as

$$\begin{aligned} Z_i &= i\frac{1}{\kappa_i}\frac{l_{\mathrm{eff}}\mathrm{Im}(Z_{\mathrm{in}})}{B}, \quad l_{\mathrm{eff}} = C\left(\frac{B}{D} - 1\right), \\ \mathrm{Im}(Z_{\mathrm{in}}) &\approx -\frac{k\eta}{2\pi}\left[\ln\left(\frac{kw}{8}\right) + \gamma\right], \end{aligned} \tag{5}$$

where $l_{\mathrm{eff}}$ is the effective length of the meander, $C$ and $D$ are the parameters of the meander [see Fig. 1(b)], and $\gamma \approx 0.5772$ is the Euler constant. The preceding expressions (5) are a rough approximation of the inductive-load-impedance density since they do not take into account the interaction between the meander strips and capacitive response to the incident wave. Geometrical parameters $w$, $B$, and $D$ are the same for all unit cells and are fixed. Parameters $A$ and $C$ are found from Eqs. (4) and (5) for each unit cell according to load-impedance densities calculated beforehand. The last step of the design procedure

is to additionally adjust parameters $A$ and $C$ by means of a parametric sweep with respect to the scaling parameters $\kappa_c$ and $\kappa_i$, which are the same for different unit cells. In contrast to the design procedure for metasurfaces, here we perform simulations of a whole supercell having $\kappa_c$ and $\kappa_i$ as the only two free parameters. This allows us to account for interaction between unit cells and immediately arrive at the ultimate design. For a more-detailed description of the design procedure, see Appendix B.

The importance of the near-field control can be demonstrated by consideration of a simple example of a nonspecular reflection at extreme angles [21,23,24]. Namely, we consider the reflection of a normally incident plane wave at an angle of 80°. In this case, there are only three propagating diffraction orders (negative first, zeroth, and positive first), as shown in Fig. 2(a). Thus, to realize anomalous reflection, one has to cancel scattering in the negative first and zeroth diffraction orders, which requires six loaded wires per supercell implemented by passive and lossless elements. The second example we consider is the splitting of the normally incident plane wave into two reflected plane waves propagating at 30° (first diffraction order) and 80° (second diffraction order). In contrast to commonly demonstrated examples of beam splitting, here

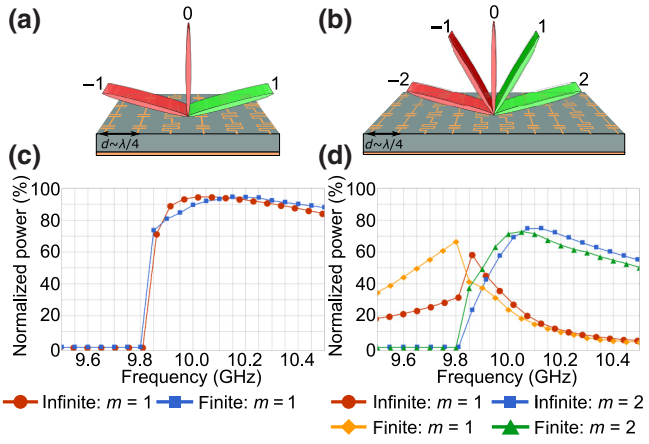


FIG. 2. Power management between propagating diffraction orders by the metagratings considered with six and eight unit cells per period: (a),(b) schematics and (c),(d) simulation data. Results for infinite and finite-size metagratings are presented. (a),(b) Excited (green lobes) and canceled (red lobes) propagating diffraction orders corresponding to the plots in (c),(d) showing the 3D full-wave simulated frequency responses of the metagratings (i.e., part of total power scattered in a given diffraction order versus frequency). (a),(c) Example of nonspecular reflection at an angle of 80° by means of a metagrating with six unit cells per period. The finite-size metagrating has 16 supercells. (b),(d) Example when of five plane waves reflected in the far field, only the first (third of total power) and second (two thirds of total power) propagating diffraction orders are excited with a metagrating having ten unit cells in a period. The finite-size metagrating has eight supercells. In both examples, normal incidence is assumed.

the incident wave power is not equally distributed between the excited diffraction orders. Particularly, we design the sample to steer one third of the total power in the first diffraction order and two thirds in the second one. This scenario is schematically depicted in Fig. 2(b), where there are five propagating diffraction orders controlled by ten loaded wires in a supercell. Other examples are provided in Sec. IV.

The two metagratings are designed to operate at 10 GHz and are tested in the following three steps. First, by means of three-dimensional (3D) full-wave simulations we test the metagrating designs in an infinite-array configuration by imposing periodic boundary conditions on a single supercell and by assuming plane-wave illumination. Figures 2(c) and 2(d) demonstrate the frequency response of the infinite metagratings. It is seen that the efficiency is above 95% in both examples considered at the frequency of operation. The remaining 5% of the power is dissipated as heat in the substrate due to dielectric losses and as spurious scattering due to imperfections of the design. In a second step, 3D full-wave simulations are used to test finite-size physical metagratings with a number of supercells corresponding to that used for fabrication of the experimental samples. To be able to further compare the results of these simulations with the experimental data, features of the experimental setup have to be taken into account. The fabricated samples are tested in an anechoic chamber dedicated to radar-cross-section bistatic measurements. Transmitting and receiving horn antennas are mounted on a common circular track of 5 m radius. A photograph of the experimental setup is shown in Fig. 6. The physical size of the experimental samples is approximately 480 mm ($y$ direction) by 160 mm ($x$ direction), as illustrated in Figs. 3(a) and 3(b). Thus, the wavefront of the incident wave in the $y$ direction cannot be approximated by a plane wave. To take this configuration into account, simulations are performed under the assumption of a cylindrical incident wave with periodic boundary conditions applied in the $x$ direction. The scattered fields are calculated on a circle enclosing the metagratings and are then extrapolated to a 5 m radius with the help of the Chu-Stratton formula [39,40]. See Appendixes C and D for details on the simulation data-processing technique. Figures 2(c) and 2(d) allow one to compare the efficiency of the finite-size metagratings with the that of the ideal case of the infinite metagratings. The discrepancy in Fig. 2(d) at low frequencies stems from disappearance of the second propagating diffraction orders, which clearly has an impact on the performance of a finite-size metagrating. However, this issue is yet to be studied. Finally, we compare the simulation results for the finite-size metasurfaces with experimental data. In the current experiment, the transmitter is fixed and the receiver moves with a 0.5° step. The minimum angle between the transmitter and the receiver for the scanning is 4°. Under this experimental-setup configuration, it is not

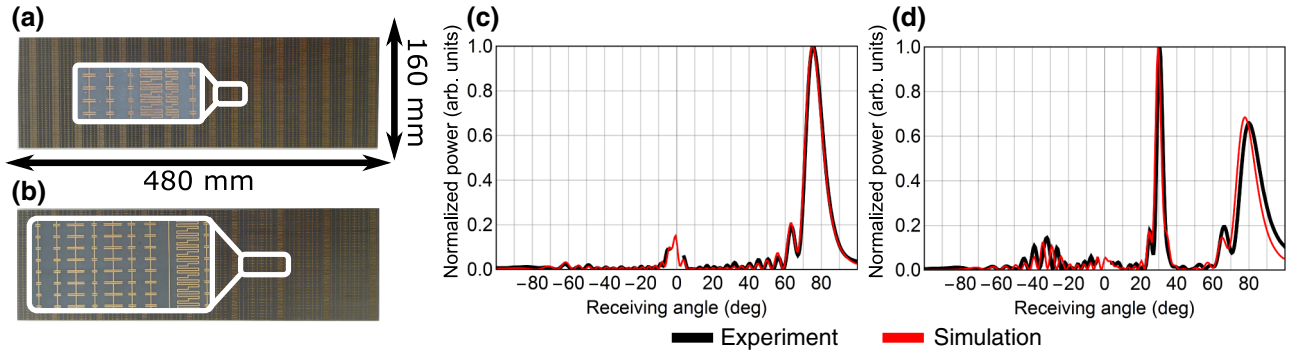


FIG. 3. Fabricated samples and comparison of the simulation and experimental data. (a),(b) Photographs of the samples performing (a) nonspecular reflection at 80° ($N = 6$) and (b) splitting into two plane waves propagating at 30° and 80° ($N = 10$). (c),(d) Experimentally measured and numerically simulated scattering patterns: (c) nonspecular reflection at 10.1 GHz (main beam has 93% of the total power) and (d) unequal splitting into two plane waves at 9.95 GHz (there is 31.5% of the total power in the first order and 63.5% in the second order).

possible to measure specular reflection in the experiment. Therefore, the performance of the fabricated samples can be estimated from the simulation data depicted in Figs. 2(c) and 2(d). Figures 3(c) and 3(d) compare the measured and simulated scattered patterns, where good agreement can be observed.

## IV. OTHER EXAMPLES BY TWO-DIMENSIONAL SIMULATIONS

So far we have demonstrated only two examples of metagratings for controlling diffraction patterns. However, the approach developed allows one to realize arbitrary diffraction patterns. Figure 4 demonstrates different configurations of the far-field scattering pattern from metagratings of two different periods. The scattering pattern is obtained by 2D full-wave simulations performed with COMSOL MULTIPHYSICS as described in Appendix E. The metagratings in Fig. 4 are designed to equally split the power of a normally incident plane wave between excited propagating diffraction orders. The numbers next to each lobe represent the part of the total power carried by a given beam. The imperfections are only due to the finite size of the metagratings in the $y$ direction (i.e., finite number

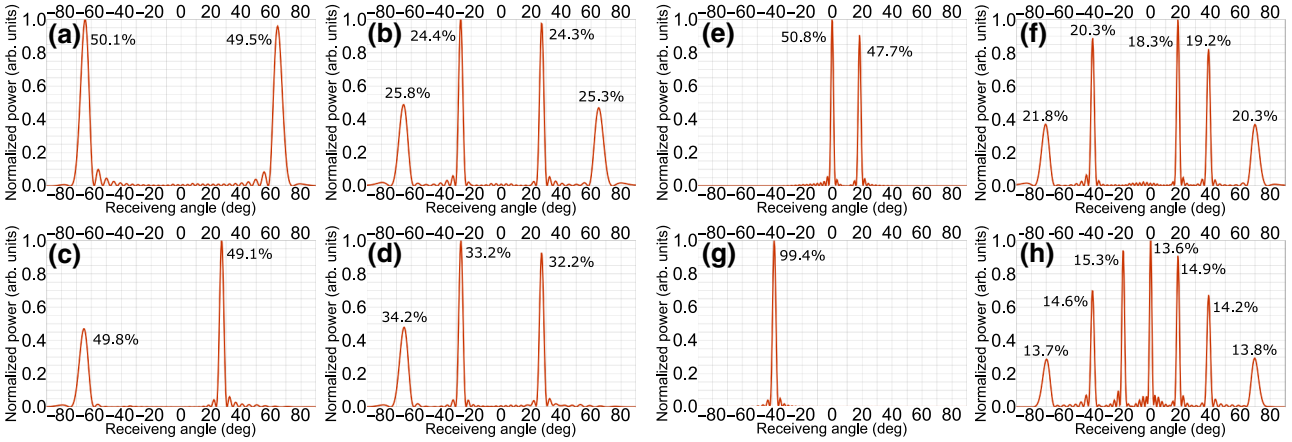


FIG. 4. Far-field scattering patterns from finite-size metagratings under normally-incident-plane-wave illumination obtained by means of 2D full-wave COMSOL MULTIPHYSICS simulations. Each finite-size metagrating has eight supercells. Numbers next to each lobe represent the part of the power in a given lobe. All examples aim to demonstrate equal distribution of the incident power between all excited propagating diffraction patterns [using Eq. (3), which assumes infinite samples]. (a)–(d) Period $L = 2 \times 30/\sin 65°$, and there are five propagating diffraction orders. (a) Negative and postive second diffraction orders are excited. (b) Negative second, negative first, positive first, and positve second diffraction orders are excited. (c) Negative second and positive first diffraction orders are excited. (d) Negative second, negative first, and positive first diffraction orders are excited. (e)–(h) Period $L = 3 \times 30/\sin 70°$, and there are seven propagating diffraction orders. (e) Zeroth and postive first diffraction orders are excited. (f) All difraction orders are excited apart from zeroth and negative first diffraction orders. (g) Only the negative second diffraction order is excited. (h) All propagating orders are excited.

of periods). Indeed, the scattering problem for finite-size objects is more complex than in the case of infinite, truly periodic structures. Strictly speaking, the theory developed is valid for finite-size metagratings only when an incident wave effectively illuminates a metagrating's area much greater than its period and much smaller than its whole size. For instance, this is the case for a Gaussian beam with waist $w_{\mathrm{GB}}$ such that $1 \ll w_{\mathrm{GB}}/L \ll N_s$ ($N_s$ is the total number of supercells).

## V. DISCUSSION AND CONCLUSION

The experimental-validation results represent extreme examples in the control of diffraction patterns that are challenging or impossible to realize by other means. For instance, to perform large-angle nonspecular reflection with a scalar reflective metasurface one has to significantly rely on numerical optimization techniques [23, 24]. Otherwise, one has to design a three-layer scalar metasurface emulating omega-bianisotropic response or a tensorial reflective metasurface [21,22]. To date, neither bianisotropic nor tensorial metasurfaces have been validated experimentally or by means of 3D full-wave simulations for nonspecular-reflection applications. On the other hand, the metagratings presented in Ref. [34] and having the number of unit cells per supercell *equal* to the number of propagating diffraction orders would demonstrate maximum efficiency of only 70% in the examples shown.

To conclude, in this paper we demonstrate that to perfectly control the diffraction pattern each propagating diffraction order requires 2 degrees of freedom represented *only* by passive and lossless loaded thin wires. Thus, a metagrating having the number of unit cells per supercell twice the number of propagating diffraction orders allows one to set arbitrary complex amplitudes of all diffracted propagating plane waves and accurately adjust the near field to satisfy the conditions of passivity and absence of loss.

Although the proof of concept is done at microwave frequencies under the assumption of TE polarization, the main theoretical result is general. Significantly decreasing the number of unit cells per wavelength (compared with metasurfaces) greatly relaxes the fabrication constraints, which makes it easier to develop metagratings operating in the optical domain and capable of controlling all propagating diffraction orders. Recently, a metagrating performing perfect refraction in the first order in the midinfrared-frequency range was fabricated and experimentally tested [41]. Control over the reflection at infrared frequencies was demonstrated in Ref. [42] by means of numerical simulations. Meanwhile, the formulas presented can be adapted for the case of TM polarization (and magnetic line currents) by means of duality relations [42,43]. For example, a unit cell possessing magnetic response can be designed on the basis of a split-ring resonator [27,42]. Moreover, recent advances in the area of manipulating acoustic wavefronts [44–47] suggest that the theory developed can be generalized also for the needs of the acoustics community.

The possibility to develop metagratings operating in different frequency ranges as well as for other domains of physics, such as acoustics, opens an avenue for a plethora of applications. Particularly, metagratings can enrich the potential implementations of efficient flat optics components and tunable microwave antennas by achieving the benefits of simple excitation, ease of fabrication, and integration.

## ACKNOWLEDGMENT

The authors acknowledge the help of Anil Cheraly (ONERA) in conducting the experiment.

## APPENDIX A: THEORY

A single electric line current $\mathbf{J}(\mathbf{r}) = I\delta(y,z)\mathbf{x}_0$ radiates a cylindrical wave with the electric field in the form of a Hankel function of the second kind of zeroth order $H_0^{(2)}[k\sqrt{y^2+z^2}]$ (see Ref. [43]):

$$E_x(y,z) = -\frac{k\eta}{4} I H_0^{(2)}[k\sqrt{y^2+z^2}], \quad E_y = E_z = 0, \tag{A1}$$

where $k = \omega\sqrt{\varepsilon\mu}$ and $\eta = \sqrt{\mu/\varepsilon}$. The electric field created by an infinite array of $N$ equidistant line currents per period $L$ is given by the following series:

$$E_x(y,z) = -\frac{k\eta}{4} \sum_{q=1}^{N} \sum_{n=-\infty}^{\infty} I_q e^{-ik\sin\theta nL} \times H_0^{(2)}[k\sqrt{(y-nL-(q-1)d)^2+z^2}], \tag{A2}$$

where the phase $\exp(-ik\sin\theta nL)$ appears because of the plane-wave illumination at angle $\theta$. The Poisson's formula applied to the series of Hankel functions ($f(nL) = \exp(-ik\sin\theta nL) H_0^{(2)}[k\sqrt{(y-nL-(q-1)d)^2+z^2}]$)

$$\sum_{n=-\infty}^{+\infty} f(nL) = \sum_{m=-\infty}^{+\infty} \int_{-\infty}^{+\infty} \frac{dw}{L} f(w) e^{-i\frac{2\pi m}{L}w} \tag{A3}$$

is used to express the series (A2) via plane waves

$$E_x(y,z) = -\frac{k\eta}{2L} \sum_{q=1}^{N} \sum_{m=-\infty}^{\infty} \frac{I_q e^{i\xi_m(q-1)d}}{\beta_m} e^{-i\xi_m y - i\beta_m|z|}. \tag{A4}$$

The Fourier transformation of the Hankel function is given by the following formula:

$$\int_{-\infty}^{+\infty} dw H_0^{(2)}[k\sqrt{(y-w)^2+z^2}] e^{-i\xi_m w} = 2\frac{e^{-i\xi_m y - i\beta_m|z|}}{\beta_m}. \tag{A5}$$

The magnetic fields corresponding to Eqs. (A1) and (A4) can be found by means of the Maxwell equations. The effect of the grounded substrate on the field radiated by the array can be derived in the same manner as in Ref. [29]. After some algebra, one arrives at Eq. (1) for the complex amplitudes of propagating and nonpropagating diffraction orders outside the substrate. The factor $R_m^{\mathrm{TE}}$ appearing in the amplitudes corresponds to the Fresnel reflection coefficient given as follows:

$$R_m^{\mathrm{TE}} = \frac{i\gamma_m^{\mathrm{TE}} \tan(\beta_m^s h) - 1}{i\gamma_m^{\mathrm{TE}} \tan(\beta_m^s h) + 1}, \quad \gamma_m^{\mathrm{TE}} = \frac{k_s \eta_s \beta_m}{k\eta \beta_m^s}, \tag{A6}$$

where $\beta_s = \sqrt{\varepsilon_s \mu_s k^2 - \xi_m^2}$ and $\eta_s = \eta\sqrt{\mu_s/\varepsilon_s}$.

Mutual-impedance densities $Z_{qp}^{(m)}$ take into consideration the interaction of the $q$th wire (located in the zeroth period) with the substrate and adjacent wires and are expressed via the following formulas:

$$\begin{aligned} Z_{qp}^{(m)} &= \frac{k\eta}{4} \sum_{n=-\infty}^{+\infty} H_0^{(2)}[k|(q-p)d - nL|] e^{-ik\sin\theta nL} \\ &\quad + \frac{k\eta}{2L} \sum_{m=-\infty}^{+\infty} e^{i\xi_m(p-q)d} \frac{R_m^{\mathrm{TE}}}{\beta_m}, \quad q \neq p, \\ Z_{qq}^{(m)} &= \frac{k\eta}{2} \sum_{n=1}^{+\infty} \cos(k\sin\theta nL) H_0^{(2)}(knL) \\ &\quad + \frac{k\eta}{2L} \sum_{m=-\infty}^{+\infty} \frac{R_m^{\mathrm{TE}}}{\beta_m}. \end{aligned} \tag{A7}$$

The series containing $R_m^{\mathrm{TE}}$ correspond to the interaction with the substrate. The electric field at the location of the $q$th wire in the zeroth period created by the rest of the $q$ wires and all other wires ($q \neq p$) is associated with the first terms constituting $Z_{qq}^{(m)}$ and $Z_{qp}^{(m)}$, respectively.

## APPENDIX B: DESIGN PROCEDURE AND PARAMETERS OF THE EXPERIMENTAL SAMPLES

The two metagratings presented as examples in the main text are designed to operate at 10 GHz ($\lambda \approx 30$ mm). To get the load-impedance densities, we start by setting the amplitudes of propagating diffraction orders. In the first case of nonspecular reflection of a normally incident plane wave at 80°, the period of the structure $L_{\mathrm{I}} = 30/\sin 80^\circ$ mm and there are three propagating diffraction orders: $A_{-1} = 0, A_0 = 0$, and $A_1 = 1/\sqrt{\cos 80^\circ}$. It requires six polarization line currents per period separated by distance $d_{\mathrm{I}} = L_{\mathrm{I}}/6$. The complex amplitudes of the three nonpropagating diffraction orders $A_{-3}$, $A_{-2}$, and $A_2$ are found by our numerically solving the system of Eq. (3). When all six amplitudes are known, we calculate the six polarization currents $I_q$ from Eq. (1). Then the load-impedance densities are found from Eq. (2). The same procedure is repeated for the other metagrating performing the splitting of the normally incident plane wave between the first propagating diffraction order (third of the power) and the second propagating diffraction order (two thirds of the power) propagating. The period of the metagrating $L_{\mathrm{II}} = 2 \times 30/\sin 80^\circ$ mm and there are ten polarization line currents separated by distance $d_{\mathrm{II}} = L_{\mathrm{II}}/10$. The complex amplitudes of the five propagating diffraction orders are set as $A_{-2} = 0$, $A_{-1} = 0$, $A_0 = 0$, $A_1 = \sqrt{\frac{1}{3}/\sqrt{1-(\lambda/L_{\mathrm{II}})^2}}$, and $A_2 = \sqrt{\frac{2}{3}/\cos 80^\circ}$. Again, the complex amplitudes of the nonpropagating diffraction orders $A_{-5}$, $A_{-4}$, $A_{-3}$, $A_3$, and $A_4$ are solutions of Eq. (3). Computed load-impedance densities can be found in Table I.

To design the experimental samples, $w$, $B$, and $D$ are fixed and kept the same for all unit cells in a metagrating, as shown in Fig. 5. For the first sample performing nonspecular anomalous reflection, $w_{\mathrm{I}} = 0.25$ mm, $B_{\mathrm{I}} = 3$ mm, and $D_{\mathrm{I}} = 0.6$ mm. In the case of the second sample used for the beam splitting, $w_{\mathrm{II}} = 0.25$ mm, $B_{\mathrm{II}} = 3.75$ mm, and $D_{\mathrm{II}} = 0.75$ mm. The substrate used is F4BM220 with $\varepsilon_s = 2.2(1 - i10^{-3})$, $\mu_s = 1$, and thickness $h = 5$ mm.

To find $A$ and $C$ of each unit cell, we use Eqs. (4) and (5) and 3D full-wave simulations of a metagrating single supercell (such as the ones in Fig. 5) with imposed periodic boundary conditions. We perform a parametric sweep with respect to the scaling parameters $\kappa_c$ and $\kappa_i$ until the model acts as desired. For the first and second samples, the optimal parameters are $\kappa_c = 0.9$ and $\kappa_i = 1.35$ and $\kappa_c = 0.92$ and $\kappa_i = 2.66$, respectively. It is important to note that the scaling parameters are independent of the unit cell. In contrast to the design procedure for metasurfaces, here we perform simulations of a whole supercell having $\kappa_c$ and $\kappa_i$ as the only two free parameters. In this way we account for

TABLE I. Parameters of metagratings presented in the main text. The indexes correspond to the numbered unit cells in Fig. 1.

| Load-impedance density ($\eta/\lambda$) | $Z_1$ | $Z_2$ | $Z_3$ | $Z_4$ | $Z_5$ | $Z_6$ | $Z_7$ | $Z_8$ | $Z_9$ | $Z_{10}$ |
|---|---|---|---|---|---|---|---|---|---|---|
| Nonspecular reflection | $-i10.6$ | $-i6.27$ | $-i12.2$ | $i12.5$ | $i22.4$ | $-i15.7$ | ... | ... | ... | ... |
| Beam splitting | $-i9.32$ | $-i6.88$ | $-i2.77$ | $-i8.57$ | $-i2.60$ | $-i6.03$ | $-i4.10$ | $i0.38$ | $i13.0$ | $-i8.98$ |
| Geometrical parameters (mm) | $A_1$ | $A_2$ | $A_3$ | $C_4$ | $C_5$ | $A_6$ | ... | ... | ... | ... |
| Nonspecular reflection | 2.0 | 3.3 | 1.7 | 2.9 | 5.2 | 1.3 | ... | ... | ... | ... |
| Geometrical parameters (mm) | $A_1$ | $A_2$ | $A_3$ | $A_4$ | $A_5$ | $A_6$ | $A_7$ | $C_8$ | $C_9$ | $A_{10}$ |
| Beam splitting | 1.7 | 2.3 | 5.6 | 1.8 | 6.0 | 2.6 | 3.8 | 0 | 7.0 | 1.7 |

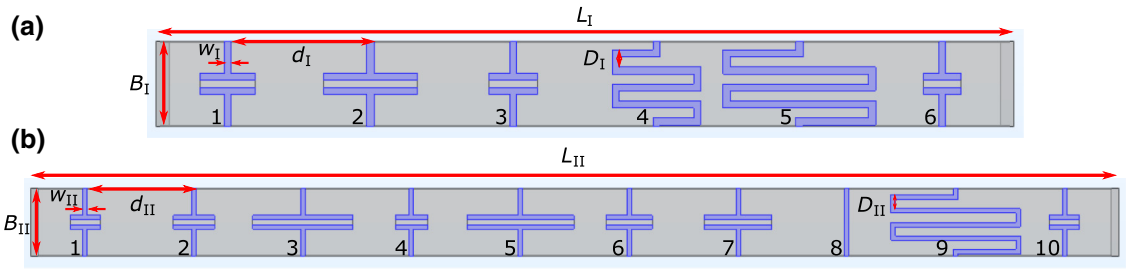


FIG. 5. Outline of the metagrating supercell geometry performing (a) nonspecular reflection at 80° and (b) beam splitting in the first (third of power) and second (two thirds of power) diffraction orders. Each unit cell of the metagratings is numbered in correspondence with the numbering in Table I.

interaction between different unit cells and immediately arrive at the ultimate design. Geometrical parameters of the fabricated samples are given in Table I.

## APPENDIX C: PROCESSING OF 3D SIMULATION DATA

In the measurement setup (see Fig. 6), the distance between the antennas and the sample is 5 m. This distance is not large enough for us to assume that the measurements are performed under the far-field condition. Indeed, the physical dimensions of the experimental samples are approximately 480 mm in the $y$ direction and 160 mm in the $x$ direction; see the photographs in Figs. 3(a) and 3(b). Thus, the wavefront of the incident wave in the $y$ direction cannot be approximated by a plane wave. To take it into account, simulations of the finite number of supercells (shown in Fig. 5) are performed by our assuming a cylindrical incident wave (phase center is 5 m away) with periodic boundary conditions applied in the $x$ direction. To correctly compare the simulation and measurement results, we harness the Chu-Stratton integration formula [39,40] to extrapolate the field calculated on the circle $C_1$ of radius 258.7 mm [illustrated by the red curve in Fig. 7(a)] to the circle $C_2$ with 5 m radius:

$$\mathbf{E}(y_2,z_2)=\frac{1}{4\pi}\oint_{C_1}\left(i\omega\mu[\hat{\mathbf{m}}\times\mathbf{H}(y_1,z_1)]+[\hat{\mathbf{m}}\times\mathbf{E}(y_1,z_1)]\times\nabla+[\hat{\mathbf{m}}\mathbf{E}(y_1,z_1)]\nabla\right)G(y_2-y_1,z_2-z_1)dl, \tag{C1}$$

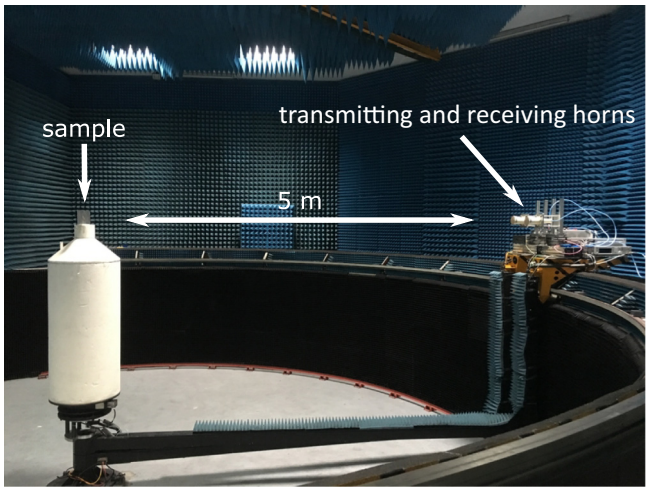


FIG. 6. Photograph of the experimental setup used to measure the scattering patterns.

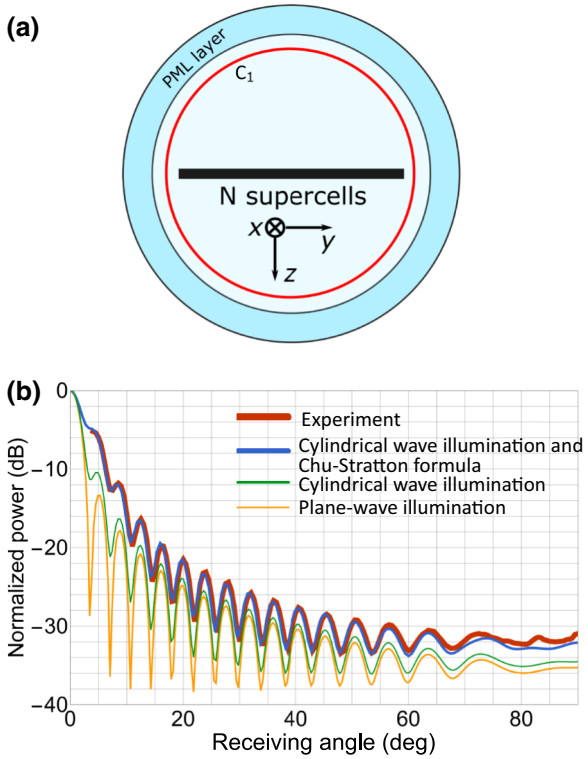


FIG. 7. (a) Two-dimensional cross section of the 3D full-wave simulation model of a finite-size metagrating. The red curve depicts the circle where the scattered fields are extracted. (b) Power-scattering pattern from a metallic plate of length 485 mm simulated numerically under different conditions and compared with the experimental curve; the frequency is 10 GHz. PML, perfectly matched layer.

where $y_2$ and $z_2$ are the coordinates of a point belonging to $C_2$, the integrand contains the fields computed on $C_1$, $G$ is the free-space Green function, and $\hat{\mathbf{m}}$ is the unit normal vector directed outward to $C_1$. As the simulations are performed with periodic boundary conditions in the $x$ direction, 2D symmetry is assumed, and thus we use $G(y,z) = iH_0^{(2)}[k\sqrt{y^2+z^2}]/4$ as a Green function.

Figure 7(b) demonstrates the importance of the Chu-Stratton formula. It compares the scattering patterns from a metallic plate measured experimentally and obtained via numerical simulations under different conditions: (i) the metallic plate is under normally-incident-plane-wave illumination and the far field is calculated; (ii) the metallic plate is under cylindrical wave illumination, the phase center is at a distance of 5 m, and the far field is calculated; (iii) the metallic plate is under cylindrical wave illumination, the scattered field is processed by means of the Chu-Stratton formula, and pattern at a distance of 5 m is built.

## APPENDIX D: CALCULATION OF THE POWER SCATTERED IN A GIVEN DIFFRACTION ORDER

The diffraction pattern appearing when a plane wave reflects from an infinite metagrating is represented by a finite number of plane waves propagating at certain angles. The power scattered in the $m$th propagating diffraction order is then calculated as $|A_m^{\mathrm{TE}}|^2\beta_m/\beta_0$ (assuming unit amplitude of the incident wave). However, for a finite-size periodic structure under plane-wave like illumination, the pattern of the scattered field is much more complex. In this case we use the following formula to estimate the part of the total power $\alpha_m(\nu)$ scattered in a given diffraction order:

$$\alpha_m(\nu) = \frac{\int_{\theta_1^m}^{\theta_2^m} P(\nu,\theta)d\theta}{\sum_{m=-l}^{r}\int_{\theta_1^m}^{\theta_2^m} P(\nu,\theta)d\theta}, \tag{D1}$$

where $P(\nu,\theta)$ represents the power scattered in the receiving angle $\theta$ and $\nu$ is the frequency. The integration is performed only over the receiving-angle range of half the maximum power of the beam corresponding to the $m$th diffraction order. The summation in the denominator includes all propagating diffraction orders at frequency $\nu$. Angles $\theta_1^m$ and $\theta_2^m$ are found as follows. First, we accurately localize the maximum of the $m$th diffraction order around the receiving angle $\sin^{-1}(\xi_m/k)$. The power corresponding to the angles $\theta_1^m$ and $\theta_2^m$ is 3 dB less than the power at the maximum.

## APPENDIX E: TWO-DIMENSIONAL FULL-WAVE SIMULATIONS OF METAGRATINGS WITH COMSOL MULTIPHYSICS

A COMSOL MULTIPHYSICS model for 2D full-wave simulations of metagratings can be built in the following way.

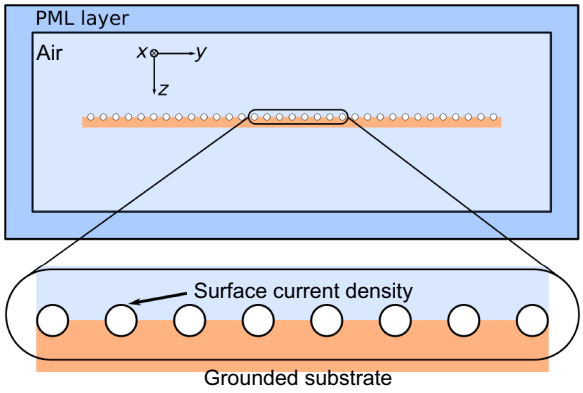


FIG. 8. The 2D COMSOL MULTIPHYSICS model used for simulating metagratings. The white regions inside the circles are excluded from the model. Polarization line currents of effective radius $r_0$ (radius of the circles, it represents the input-impedance density) are simulated as surface current density: $\mathbf{J}_{es} = E_x/Z_q/(2\pi r_0)\hat{\mathbf{x}}_0$ ($\hat{\mathbf{x}}_0$ is the unit vector in the $x$ direction). The total number of line currents (circles) is the number of line currents per period times the number of periods. PML, perfectly matched layer.

The principal element of a metagrating is a polarization line current that is modeled in COMSOL MULTIPHYSICS as surface current density assigned to the boundary of a circle, as shown in Fig. 8. The radius of the circle $r_0$ should be equal to the effective radius of a thin wire to get the correct value of the input-impedance density. It is important to exclude from the model the interior of the circles, otherwise one would get an incorrect value of the input-impedance density. The surface current density $\mathbf{J}_{es}$ is set as follows: $E_x/Z_q/(2\pi r_0)\hat{\mathbf{x}}_0$ ($Z_q$ is the load-impedance density of the $q$th thin wire). The array of circles is placed on a PEC-backed substrate (the circles' centers are on the top of the substrate) as shown in Fig. 8. To excite the model, we use a scattered-field formulation and set a background field. The rest of the model is standard and can be understood from Fig. 8.

[1] R. W. Wood, The echelette grating for the infra-red, The London, Edinburgh, and Dublin Philos. Mag. J. Sci. **20**, 770 (1910).
[2] Henry A. Rowland, Gratings in theory and practice, The London, Edinburgh, and Dublin Philos. Mag. J. Sci. **35**, 397 (1893).
[3] R. F. Stamm and J. J. Whalen, Energy distribution of diffraction gratings as a function of groove form (calculations by an equation of henry a. rowland), JOSA **36**, 2 (1946).
[4] M. Breidne, S. Johansson, L.-E. Nilsson, and H. Åhlèn, Blazed holographic gratings, Optica Acta: Int. J. Opt. **26**, 1427 (1979).

[5] A. Hessel, J. Schmoys, and D. Y. Tseng, Bragg-angle blazing of diffraction gratings∗, J. Opt. Soc. Am. **65**, 380 (1975).

[6] M. Breidne and D. Maystre, Perfect blaze in non-littrow mountings, Optica Acta: Int. J. Opt. **28**, 1321 (1981).

[7] D. M. Pozar, Flat lens antenna concept using aperture coupled microstrip patches, Electron. Lett. **32**, 2109 (1996).

[8] J. Huang and J. A. Encinar, *Reflectarray Antennas* (John Wiley & Sons, Hoboken, New Jersey, 2007), Vol. 30.

[9] D. M. Pozar, Wideband reflectarrays using artificial impedance surfaces, Electron. Lett. **43**, 148 (2007).

[10] S. Jahani and Z. Jacob, All-dielectric metamaterials, Nat. Nanotech. **11**, 23 (2016).

[11] S. B. Glybovski, S. A. Tretyakov, P. A. Belov, Y. S. Kivshar, and C. R. Simovski, Metasurfaces: From microwaves to visible, Phys. Rep. **634**, 1 (2016).

[12] K. Sun, R. Fan, X. Zhang, Z. Zhang, Z. Shi, N. Wang, P. Xie, Z. Wang, G. Fan, H. Liu, C. Liu, T. Li, C. Yan, and Z. Guo, An overview of metamaterials and their achievements in wireless power transfer, J. Mater. Chem. C **6**, 2925 (2018).

[13] X. C. Tong, *Functional Metamaterials and Metadevices* (Cham, Springer, 2018).

[14] N. Yu, P. Genevet, M. A. Kats, F. Aieta, J.-P. Tetienne, F. Capasso, and Z. Gaburro, Light propagation with phase discontinuities: Generalized laws of reflection and refraction, Science **334**, 333 (2011).

[15] C. Pfeiffer and A. Grbic, Metamaterial Huygens' Surfaces: Tailoring Wave Fronts with Reflectionless Sheets, Phys. Rev. Lett. **110**, 1 (2013).

[16] V. S. Asadchy, M. Albooyeh, S. N. Tcvetkova, A. Díaz-Rubio, Y. Ra'di, and S. A. Tretyakov, Perfect control of reflection and refraction using spatially dispersive metasurfaces, Phys. Rev. B **94**, 075142 (2016).

[17] V. S. Asadchy, A. Díaz-Rubio, S. N. Tcvetkova, D.-H. Kwon, A. Elsakka, M. Albooyeh, and S. A. Tretyakov, Flat Engineered Multichannel Reflectors, Phys. Rev. X **7**, 031046 (2017).

[18] A. Epstein and G. V. Eleftheriades, Arbitrary power-conserving field transformations with passive lossless omega-type bianisotropic metasurfaces, IEEE. Trans. Antennas Propag. **64**, 3880 (2016).

[19] M. Chen, E. Abdo-Sánchez, A. Epstein, and G. V. Eleftheriades, Theory, design, and experimental verification of a reflectionless bianisotropic huygens' metasurface for wide-angle refraction, Phys. Rev. B **97**, 125433 (2018).

[20] G. Lavigne, K. Achouri, V. S. Asadchy, S. A. Tretyakov, and C. Caloz, Susceptibility derivation and experimental demonstration of refracting metasurfaces without spurious diffraction, IEEE. Trans. Antennas Propag. **66**, 1321 (2018).

[21] A. Epstein and G. V. Eleftheriades, Synthesis of Passive Lossless Metasurfaces using Auxiliary Fields for Reflectionless Beam Splitting and Perfect Reflection, Phys. Rev. Lett. **117**, 256103 (2016).

[22] D.-H. Kwon and S. A. Tretyakov, Perfect reflection control for impenetrable surfaces using surface waves of orthogonal polarization, Phys. Rev. B **96**, 085438 (2017).

[23] A. Díaz-Rubio, V. S. Asadchy, A. Elsakka, and S. A. Tretyakov, From the generalized reflection law to the realization of perfect anomalous reflectors, Sci. Adv. **3**, e1602714 (2017).

[24] D. Kwon, Lossless scalar metasurfaces for anomalous reflection based on efficient surface field optimization, IEEE. Antennas Wirel. Propag. Lett. **17**, 1149 (2018).

[25] F. Monticone, N. M. Estakhri, and A. Alù, Full Control of Nanoscale Optical Transmission with a Composite Metascreen, Phys. Rev. Lett. **110**, 203903 (2013).

[26] A. Epstein and G. V. Eleftheriades, Floquet-Bloch analysis of refracting Huygens metasurfaces, Phys. Rev. B: Condens. Matter Mater. Phys. **90**, 1 (2014).

[27] Y. Ra'di, D. L. Sounas, and A. Alù, Metagratings: Beyond the Limits of Graded Metasurfaces for Wave Front Control, Phys. Rev. Lett. **119**, 067404 (2017).

[28] A. Epstein and O. Rabinovich, Unveiling the Properties of Metagratings via a Detailed Analytical Model for Synthesis and Analysis, Phys. Rev. Appl. **8**, 054037 (2017).

[29] O. Rabinovich and A. Epstein, Analytical design of printed circuit board (pcb) metagratings for perfect anomalous reflection, IEEE. Trans. Antennas Propag. **66**, 4086 (2018).

[30] A. Epstein and O. Rabinovich, Perfect anomalous refraction with metagratings, arXiv:1804.02362 (2018).

[31] O. Rabinovich, I. Kaplon, J. Reis, and A. Epstein, Experimental demonstration and in-depth investigation of analytically designed anomalous reflection metagratings, arXiv:1809.01938 (2018).

[32] A. M. H. Wong and G. V. Eleftheriades, Perfect Anomalous Reflection with a Bipartite Huygens' Metasurface, Phys. Rev. X **8**, 011036 (2018).

[33] A. M. H. Wong, P. Christian, and G. V. Eleftheriades, Binary huygens' metasurfaces: Experimental demonstration of simple and efficient near-grazing retroreflectors for te and tm polarizations, IEEE. Trans. Antennas Propag. **66**, 2892 (2018).

[34] V. Popov, F. Boust, and S. N. Burokur, Controlling Diffraction Patterns with Metagratings, Phys. Rev. Appl. **10**, 011002 (2018).

[35] S. Tretyakov, *Analytical Modeling in Applied Electromagnetics* (Artech House, Norwood, MA, 2003).

[36] O. Luukkonen, C. Simovski, G. Granet, G. Goussetis, D. Lioubtchenko, A. V. Raisanen, and S. A. Tretyakov, Simple and accurate analytical model of planar grids and high-impedance surfaces comprising metal strips or patches, IEEE. Trans. Antennas Propag. **56**, 1624 (2008).

[37] X. C. Wang, A. Díaz-Rubio, A. Sneck, A. Alastalo, T. Mäkelä, J. Ala-Laurinaho, J. F. Zheng, A. V. Räisänen, and S. A. Tretyakov, Systematic design of printable metasurfaces: Validation through reverse-offset printed millimeter-wave absorbers, IEEE. Trans. Antennas Propag. **66**, 1340 (2018).

[38] X.-C. Wang, A. Díaz-Rubio, V. S. Asadchy, and S. A. Tretyakov, Reciprocal angle-asymmetric absorbers: Concept and design, arXiv:1801.09397 (2018).

[39] J. A. Stratton and L. J. Chu, Diffraction theory of electromagnetic waves, Phys. Rev. **56**, 99 (1939).

[40] J. A. Stratton, *Electromagnetic Theory* (John Wiley & Sons, Hoboken, New Jersey, 2007).

[41] Z. Fan, M. R. Shcherbakov, M. Allen, J. Allen, B. Wenner, and G. Shvets, Perfect diffraction with multiresonant bianisotropic metagratings, ACS Photonics **5**, 4303 (2018).

[42] V. Popov, M. Yakovleva, F. Boust, and S. N. Burokur, Designing metagratings via local periodic approximation: From microwaves to infrared, arXiv:1812.10164 (2018) [physics.app-ph].

[43] L. B. Felsen and N. Marcuvitz, *Radiation and Scattering of Waves* (IEEE Press, New York, 1994). Vol. 31.

[44] Y. Li, X. Jiang, R. Li, B. Liang, X. Zou, L. Yin, and J. Cheng, Experimental Realization of Full Control of Reflected Waves with Subwavelength Acoustic Metasurfaces, Phys. Rev. Appl. **2**, 064002 (2014).

[45] J. Li, C. Shen, A. Díaz-Rubio, S. A. Tretyakov, and S. A. Cummer, Systematic design and experimental demonstration of bianisotropic metasurfaces for scattering-free manipulation of acoustic wavefronts, Nat. Commun. **9**, 1342 (2018).

[46] D. Torrent, Acoustic anomalous reflectors based on diffraction grating engineering, Phys. Rev. B **98**, 060101 (2018).

[47] P. Packo, A. N. Norris, and D. Torrent, Inverse Grating Problem: Efficient Design of Anomalous Flexural Wave Reflectors and Refractors, Phys. Rev. Appl. **11**, 014023 (2019).